

PARTICLE INTERFEROMETRY: NEW THEORETICAL RESULTS

Ulrich Heinz

*Institut für Theoretische Physik, Universität Regensburg,
D-93040 Regensburg, Germany*

By measuring hadronic single-particle spectra and two-particle correlations in heavy-ion collisions, the size and dynamical state of the collision fireball at freeze-out can be reconstructed. I discuss the relevant theoretical methods and their limitations. By applying the formalism to recent pion correlation data from Pb+Pb collisions at CERN we demonstrate that the collision zone has undergone strong transverse growth before freeze-out (by a factor 2-3 in each direction), and that it expands both longitudinally and transversally. From the thermal and flow energy density at freeze-out the energy density at the onset of transverse expansion can be estimated from conservation laws. It comfortably exceeds the critical value for the transition to color deconfined matter.

1 Introduction

In the last few years a large body of evidence has been accumulated that the hot and dense collision region in ultrarelativistic heavy ion collisions thermalizes and shows collective dynamical behaviour. This evidence is based on a comprehensive analysis of the hadronic single particle spectra. It was shown that all available data on hadron production in heavy ion collisions at the AGS and the SPS can be understood within a simple model which assumes locally thermalized momentum distributions at freeze-out, superimposed by collective hydrodynamical expansion in both the longitudinal and transverse directions.^{1,2} The collective dynamical behaviour in the transverse direction is reflected by a characteristic dependence of the inverse slope parameters of the m_{\perp} -spectra ("effective temperatures") at small m_{\perp} on the hadron masses.¹ New data from the Au+Au and Pb+Pb systems³ support this picture and show that the transverse collective dynamics is much more strongly exhibited in larger collision systems than in the smaller ones from the first rounds of experiments. The amount of transverse flow also appears to increase monotonically with collision energy from GSI/SIS to AGS energies, but may show signs of saturation at the even higher SPS energy.³

The extraction of flow velocities and thermal freeze-out temperatures from the measured single particle spectra relies heavily on model assumptions.¹ There have been alternative suggestions to explain the observed features of the hadron spectra without invoking hydro-flow.^{4,5} The single-particle spectra

are ambiguous because they contain no direct information on the space-time structure and the space-momentum correlations induced by collective flow. In terms of the phase-space density at freeze-out (“emission function”) $S(x, p)$ the single-particle spectrum is given by $E dN/d^3p = \int d^4x S(x, p)$; the space-time information in S is completely washed out by integration. Thus, on the single-particle level, comprehensive model studies are required to show that a simple hydrodynamical model with only a few thermodynamic and collective parameters can fit all the data, and additional consistency checks are needed to show that the extracted fit parameter values lead to an internally consistent theoretical picture. The published literature abounds with examples demonstrating that without such consistency checks the theoretical ambiguity of the single particle spectra is nearly infinite.

This is the point where Bose-Einstein correlations between the momenta of identical particle pairs provide crucial new input. They give direct access to the space-time structure of the source *and* its collective dynamics. In spite of some remaining model dependence the set of possible model sources can thus be reduced dramatically. The two-particle correlation function $C(q, K)$ is usually well approximated by a Gaussian in the relative momentum q whose width parameters are called “HBT (Hanbury Brown-Twiss) radii”. It was recently shown^{6,7,8} that these radius parameters measure certain combinations of the second central space-time moments of the source. In general they mix the spatial and temporal structure of the source in a nontrivial way,⁷ and the remaining model dependence enters when trying to unfold these aspects.

Collective dynamics of the source leads to a dependence of the HBT radii on the pair momentum K ; this has been known for many years,^{9,10} but was recently quantitatively reanalyzed, both analytically^{7,8,11,12} and numerically.^{13,14} The velocity gradients associated with collective expansion lead to a dynamical decoupling of different source regions in the correlation function, and the HBT radii measure the size of the resulting “space-time regions of homogeneity” of the source^{10,11} around the point of maximum emissivity for particles with the measured momentum K . The velocity gradients are smeared out by a thermal smearing factor arising from the random motion of the emitters around the fluid velocity.⁷ Due to the exponential decrease of the Maxwell-Boltzmann distribution, this smearing factor shrinks with increasing transverse momentum K_\perp of the pair, which is the basic reason for the K_\perp -dependence of the HBT radii.

Unfortunately, other gradients in the source (for example spatial and temporal temperature gradients) can also generate a K -dependence of the HBT radii.^{7,12} Furthermore, the pion spectra in particular are affected by resonance

decay contributions, but only at small K_\perp . This may also affect the HBT radii in a K_\perp -dependent way.^{15,16} The isolation of collective flow, in particular transverse flow, from the K_\perp -dependence of the HBT radii thus requires a careful study of these different effects.

Our group studied this K -dependence of the HBT radii within a simple analytical model for a finite thermalized source which expands both longitudinally and transversally. For presentation I use the Yano-Koonin-Podgoretskii (YKP) parametrization of the correlator which, for sources with dominant longitudinal expansion, provides an optimal separation of the spatial and temporal aspects of the source.^{8,14} The YKP radius parameters are independent of the longitudinal velocity of the observer frame. Furthermore, in all thermal models without transverse collective flow, they show perfect M_\perp -scaling (in the absence of resonance decay contributions). Only the transverse gradients induced by a non-zero transverse flow can break this M_\perp -scaling, causing an explicit dependence on the particle rest mass. This allows for a rather model-independent identification of transverse flow from accurate measurements of the YKP correlation radii for pions and kaons. High-quality data should also allow to control the effects from resonance decays.

Due to space limitations, I will be selective with equations, figures and references. A comprehensive and didactical discussion of the formalism and a more extensive selection of numerical examples can be found in the lecture notes¹⁷ to which I refer the reader for more details.

2 Spectra and emission function

2.1 Single-particle spectra and two-particle correlations

The covariant single- and two-particle distributions are defined by

$$P_1(\mathbf{p}) = E \frac{dN}{d^3p} = E \langle \hat{a}_\mathbf{p}^+ \hat{a}_\mathbf{p} \rangle, \quad (1)$$

$$P_2(\mathbf{p}_a, \mathbf{p}_b) = E_a E_b \frac{dN}{d^3p_a d^3p_b} = E_a E_b \langle \hat{a}_{\mathbf{p}_a}^+ \hat{a}_{\mathbf{p}_b}^+ \hat{a}_{\mathbf{p}_b} \hat{a}_{\mathbf{p}_a} \rangle, \quad (2)$$

where $\hat{a}_\mathbf{p}^+$ ($\hat{a}_\mathbf{p}$) creates (destroys) a particle with momentum \mathbf{p} . The angular brackets denote an ensemble average,

$$\langle \hat{O} \rangle = \text{tr}(\hat{\rho} \hat{O}), \quad (3)$$

where $\hat{\rho}$ is the density operator associated with the ensemble. (When talking about an ensemble we may think of either a single large, thermalized source,

or a large number of similar, but not necessarily thermalized collision events.) The single-particle spectrum is normalized to the average number of particles, $\langle N \rangle$, per collision,

$$\int \frac{d^3 p}{E} P_1(\mathbf{p}) = \langle N \rangle, \quad (4)$$

while the two-particle distribution is normalized to the number of particles in pairs, $\langle N(N-1) \rangle$, per event:

$$\int \frac{d^3 p_a}{E_a} \frac{d^3 p_b}{E_b} P_2(\mathbf{p}_a, \mathbf{p}_b) = \langle N(N-1) \rangle. \quad (5)$$

The two-particle correlation function is defined as

$$C(\mathbf{p}_a, \mathbf{p}_b) = \frac{P_2(\mathbf{p}_a, \mathbf{p}_b)}{P_1(\mathbf{p}_a)P_1(\mathbf{p}_b)}. \quad (6)$$

If the two particles are emitted independently and final state interactions are neglected one can prove¹⁷ a generalized Wick theorem

$$C(\mathbf{p}_a, \mathbf{p}_b) = 1 \pm \frac{|\langle \hat{a}_{\mathbf{p}_a}^+ \hat{a}_{\mathbf{p}_b} \rangle|^2}{\langle \hat{a}_{\mathbf{p}_a}^+ \hat{a}_{\mathbf{p}_a} \rangle \langle \hat{a}_{\mathbf{p}_b}^+ \hat{a}_{\mathbf{p}_b} \rangle}. \quad (7)$$

Note that the second term is positive definite, i.e. the correlation function cannot, for example, oscillate around unity. This is no longer true if final state interactions are included (see below).

From now on I will assume that the emitted particles are bosons, and for convenience I will call them pions, although nearly everything below applies equally well to other bosonic particles.

2.2 Source Wigner function and spectra

In the language of the covariant current formalism¹⁸ the source of the emitted pions can be described in terms of classical currents $J(x)$ which act as classical sources of freely propagating pions. These currents represent a parametrization of the last collision from which the free outgoing pion emerges. Very helpful for the following will be the so-called “emission function” $S(x, K)$.^{9,19}

$$S(x, K) = \int \frac{d^4 y}{2(2\pi)^3} e^{-iK \cdot y} \langle J^*(x + \frac{1}{2}y) J(x - \frac{1}{2}y) \rangle. \quad (8)$$

It is the Wigner transform of the density matrix associated with the classical source amplitudes $J(x)$. This Wigner density is a quantum mechanical object

defined in phase-space (x, K) ; in general it is real but not positive definite. But, when integrated over x or K it yields the classical (positive definite and real) source density in momentum or coordinate space, respectively, in exactly the same way as a classical phase-space density would behave. Furthermore, textbooks on Wigner functions show that their non-positivity is a genuine quantum effect resulting from the uncertainty relation and are concentrated at short phase-space distances; when the Wigner function is averaged over phase-space volumes which are large compared to the volume $(2\pi\hbar)^3$ of an elementary phase-space cell, the result is real and positive definite and behaves exactly like a classical phase-space density.

The emission function $S(x, K)$ is thus the quantum mechanical analogue of the classical phase-space distribution which gives the probability of finding at point x a source which emits free pions with momentum K . It allows to express the single-particle spectra and two-particle correlation function via the following fundamental relations:^{9,19,20}

$$E_p \frac{dN}{d^3p} = \int d^4x S(x, p), \quad (9)$$

$$C(\mathbf{q}, \mathbf{K}) = 1 + \frac{|\int d^4x S(x, K) e^{iq \cdot x}|^2}{\int d^4x S(x, K + \frac{1}{2}q) \int d^4x S(x, K - \frac{1}{2}q)}. \quad (10)$$

For the single-particle spectrum (9), the Wigner function $S(x, p)$ on the r.h.s. must be evaluated on-shell, i.e. at $p^0 = E_p = \sqrt{m^2 + \mathbf{p}^2}$. For the correlator (10) we have defined the relative momentum $\mathbf{q} = \mathbf{p}_a - \mathbf{p}_b$, $q^0 = E_a - E_b$ between the two particles in the pair, and the total momentum of the pair $\mathbf{K} = (\mathbf{p}_a + \mathbf{p}_b)/2$, $K^0 = (E_a + E_b)/2$. Of course, since the 4-momenta $p_{a,b}$ of the two measured particles are on-shell, $p_i^0 = E_i = \sqrt{m^2 + \mathbf{p}_i^2}$, the 4-momenta q and K are in general off-shell. They satisfy the orthogonality relation

$$q \cdot K = 0. \quad (11)$$

Thus, the Wigner function on the r.h.s. of Eq. (10) is *not* evaluated at the on-shell point $K^0 = E_K$. This implies that for the correlator, in principle, we need to know the off-shell behaviour of the emission function, i.e. the quantum mechanical structure of the source. Obviously, this makes the problem appear rather untractable!

Fortunately, nature is nice to us: the interesting behaviour of the correlator (its deviation from unity) is concentrated at small values of $|\mathbf{q}|$. Expanding $K^0 = (E_a + E_b)/2$ for small q one finds

$$K^0 = E_K \left(1 + \frac{\mathbf{q}^2}{8E_K^2} + \mathcal{O}\left(\frac{\mathbf{q}^4}{E_K^4}\right) \right) \approx E_K. \quad (12)$$

Since the relevant range of q is given by the inverse size of the source (more properly: the inverse size of the regions of homogeneity in the source – see below), the validity of this approximation is ensured in practice as long as the Compton wavelength of the particles is small compared to this “source size”. For the case of pion, kaon, or proton interferometry for heavy-ion collisions this is true automatically due to the rest mass of the particles: even for pions at rest, the Compton wavelength of 1.4 fm is comfortably smaller than any typical nuclear source size. This is of enormous practical importance because it allows you essentially to replace the source Wigner density by a classical phase-space distribution function for on-shell particles. This provides a necessary theoretical foundation for the calculation of HBT correlations from classical hydrodynamic or kinetic (e.g. cascade or molecular dynamics) simulations of the collision.

If the single-particle spectrum is an exponential function of the energy then it is easy to prove⁷ that one can replace the product of single-particle distributions in the denominator of (10) by the square of the single-particle spectrum evaluated at the average momentum K :

$$C(\mathbf{q}, \mathbf{K}) \approx 1 + \left| \frac{\int d^4x e^{iq \cdot x} S(x, K)}{\int d^4x S(x, K)} \right|^2 \equiv 1 + |\langle e^{iq \cdot x} \rangle|^2. \quad (13)$$

The deviations from this approximation are proportional to the curvature of the single-particle distribution in logarithmic representation.⁷ They are small in practice because the measured single-particle spectra are usually more or less exponential. In the second equality of (13) we defined $\langle \dots \rangle$ as the average taken with the emission function; due to the K -dependence of $S(x, K)$ this average is a function of K . This notation will be used extensively in the following.

The fundamental relations (9) and (10) resp. (13) show that *both the single-particle spectrum and the two-particle correlation function can be expressed as simple integrals over the emission function*. The emission function thus is the crucial ingredient in the theory of HBT interferometry: if it is known, the calculation of one- and two-particle spectra is straightforward (even if the evaluation of the integrals may in some cases be technically involved); more interestingly, measurements of the one- and two-particle spectra provide access to the emission function and thus to the space-time structure of the source. This latter aspect is, of course, the motivation for exploiting HBT in practice. In my talk I will concentrate on the question to what extent this access to the space-time structure from only momentum-space data really works, whether it is complete, and (since we will find it is not and HBT analyses will thus be necessarily model-dependent) what can be reliably said about the

extension and dynamical space-time structure of the source anyhow, based on a minimal set of intuitive and highly suggestive model assumptions.

2.3 Final state interactions (FSI)

Equation (10) reflects the absence of final state interactions (free propagation after emission) by the appearance of the plane wave factor $e^{iq \cdot x}$ under the integral of the exchange term in the two-particle cross section:

$$P_2(\mathbf{p}_a, \mathbf{p}_b) = \int d^4x_1 d^4x_2 \left[S(x_1, K + \frac{q}{2}) S(x_2, K - \frac{q}{2}) \pm e^{iq \cdot (x_1 - x_2)} S(x_1, K) S(x_2, K) \right]. \quad (14)$$

In practice particle interferometry is done with charged particle pairs which suffer a long-range Coulomb final state repulsion on their way out to the detector. In addition, there may be strong final state interactions, e.g. in proton-proton interferometry where there is a strong s -wave resonance just above the two-particle threshold. In this case Eq. (14) must be replaced by²¹

$$P_2(\mathbf{p}_a, \mathbf{p}_b) = \int d^4x d^4y S(x + \frac{y}{2}, p_a) S(x - \frac{y}{2}, p_b) \times \left[\theta(y^0) |\phi_{\mathbf{q}/2}(\mathbf{y} - \mathbf{v}_b y^0)|^2 + \theta(-y^0) |\phi_{\mathbf{q}/2}(\mathbf{y} - \mathbf{v}_a y^0)|^2 \right] \pm \int d^4x d^4y S(x + \frac{y}{2}, K) S(x - \frac{y}{2}, K) \times \phi_{-\mathbf{q}/2}^*(\mathbf{y} - \mathbf{v} y^0) \phi_{\mathbf{q}/2}(\mathbf{y} - \mathbf{v} y^0). \quad (15)$$

Here $\mathbf{v} = \mathbf{K}/E_K$, $\mathbf{v}_a = \mathbf{p}_a/E_K$, $\mathbf{v}_b = \mathbf{p}_b/E_K$ are (to quadratic accuracy in q) the velocities of the particles with momentum \mathbf{K} , \mathbf{p}_a , \mathbf{p}_b , respectively, and $\phi_{\mathbf{q}/2}(\mathbf{r})$ is an FSI distorted wave with asymptotic relative momentum $\mathbf{q}/2$, evaluated at the two-particle relative distance \mathbf{r} . Upon replacing the latter by plane waves (15) turns into (14). The FSI distorted waves can be calculated by solving a non-relativistic Schrödinger equation for the relative motion which includes the FSI potential *in the rest system of the pair* (where $\mathbf{K} = \mathbf{v} = 0$). Eq. (15) represents a non-relativistic Galilei-transformation of the result from the pair rest frame to the frame in which \mathbf{p}_a and \mathbf{p}_b are measured; therefore it is only valid in observer frames in which the pair moves non-relativistically. In order to evaluate Eq. (15) one must therefore first transform the 4-momenta $p_{a,b}$ to such a frame (best directly into the pair rest frame). The momentum argument \mathbf{q} of the FSI distorted waves ϕ is then the difference between the two spatial momenta *in that frame*, and their space-time argument $\mathbf{y} - \mathbf{v}_i y^0$ is the

relative distance of the two particles in that frame *at the time when the second particle is emitted*.²¹ Since the latter depends not only on the time difference y^0 between emission points, but also on the velocity of the first emitted particle, these arguments depend on the momentum argument of the emission function associated with the first emitted particle. The two terms $\sim \theta(\pm y^0)$ in the direct term reflect the two possible time orderings between the emission points.

2.4 Implementation in event generators

Equations (14) and (15) can be implemented into event generators, following the procedure given in.^{21,22}

For the *direct term* one selects all pairs (i, j) with $p_i = p_a$, $p_j = p_b$ within a given numerical accuracy (bin width) which is essentially dictated by event statistics. Each pair is multiplied with a weight given by the corresponding probability density $|\phi_{\mathbf{q}/2}|^2$ of the FSI distorted wave. The latter must be evaluated in a frame in which the pair moves non-relativistically, best in the pair rest frame where $\mathbf{K} = (\mathbf{p}_a + \mathbf{p}_b)/2 = 0$. (Then $E_K = m$, and the velocities $\mathbf{v}, \mathbf{v}_{a,b}$ reduce to their usual nonrelativistic definition.) From the space-time coordinates x_i, x_j of the pair in the event generator frame one calculates the distance \mathbf{y}_{ij}^* between the two particles in the pair rest frame at the time when the second particle is produced. One then computes $|\phi_{\mathbf{q}^*/2}(\mathbf{y}_{ij}^*)|^2$ and weights the selected pair (i, j) with this number. In this expression \mathbf{q}^* is the spatial relative momentum between the two particles in the pair rest frame which must be computed from p_a, p_b in the event generator frame. In the absence of FSI, the corresponding weight is simply 1. The complete direct term is obtained by summing over all such pairs.

For the *exchange term*, the selection of pairs and weights is a little less intuitive.²² One selects all pairs (i, j) with $p_i = p_j = K$ (i.e. *on-shell particles* (!) with $\mathbf{p}_i = \mathbf{p}_j = \mathbf{K}$ and $E_i = E_j = E_K$), again within the same numerical accuracy (bin width) as above. From the production coordinates x_i, x_j one again computes the spatial distance \mathbf{y}_{ij}^* between the two particles in the pair at the time of emission of the second one, in the pair rest frame $\mathbf{K} = 0$. This distance is used to compute the weight $\phi_{-\mathbf{q}^*/2}^*(\mathbf{y}_{ij}^*)\phi_{\mathbf{q}^*/2}^*(\mathbf{y}_{ij}^*)$ for this pair. The value of \mathbf{q}^* here is *the same as above in the direct term*, i.e. it is computed from p_a and p_b by transforming into the pair rest frame, not from $p_i = p_j = K$. Without FSI, the corresponding weight²² is $\cos(\mathbf{q}^* \cdot \mathbf{y}_{ij}^*)$. The full exchange term is obtained by summing over all such pairs. Note that this selection of pairs and weights differs from previously applied algorithms which were shown²² to yield wrong results for sources with very strong x - p correlations.

Finally one must normalize the correlator by the product of single particle

spectra,

$$P_1(\mathbf{p}_a) P_1(\mathbf{p}_b) = \int d^4x S(x, p_a) \int d^4y S(y, p_b). \quad (16)$$

This normalization is best obtained from the pairs selected for the direct term above by multiplying them with unit weights.

One may object to the use of event generators for the emission function because they fix particle momenta and coordinates simultaneously and thus violate the uncertainty principle. One can generate from an event generator a quantum mechanically consistent Wigner density $S(x, p)$ by folding the event generator output with minimum uncertainty wave packets.²² The corresponding quantum mechanically consistent algorithm²² for computing single- and two-particle spectra is easily generalized to include FSI effects, by simply replacing the factors 1 and $\cos(\mathbf{q}^* \cdot \mathbf{y}_{ij}^*)$ in the direct and exchange terms, respectively, by the correct FSI weights as discussed above.

At this point I will drop the discussion of final state interactions; the rest of the lecture will deal only with the case of free particles, assuming (carelessly) that appropriate Coulomb corrections of the data have already been done by the experimentalists.

2.5 The mass-shell constraint

Expressions (10,13) show that the correlation function is related to the emission function by a Fourier transformation. At first sight this might suggest that one should easily be able to reconstruct the emission function from the measured correlation function by inverse Fourier transformation, the single particle spectrum (9) providing the normalization. This is, however, not correct. The reason is that, since the correlation function is constructed from the on-shell momenta of the measured particle pairs, not all four components of the relative momentum q occurring on the r.h.s. of (13) are independent. They are related by the “mass-shell constraint” (11) which can, for instance, be solved for q^0 :

$$q^0 = \boldsymbol{\beta} \cdot \mathbf{q} \quad \text{with} \quad \boldsymbol{\beta} = \frac{\mathbf{K}}{K^0} \approx \frac{\mathbf{K}}{E_K}. \quad (17)$$

$\boldsymbol{\beta}$ is (approximately) the velocity of the c.m. of the particle pair. The Fourier transform in (13) is therefore not invertible, and the reconstruction of the space-time structure of the source from HBT measurements will thus always require additional model assumptions.

It is instructive to insert (17) into (13):

$$C(\mathbf{q}, \mathbf{K}) \approx 1 + \left| \frac{\int d^4x \exp(i\mathbf{q}\cdot(\mathbf{x} - \boldsymbol{\beta}t)) S(x, K)}{\int d^4x S(x, K)} \right|^2. \quad (18)$$

This shows that the correlator $C(\mathbf{q}, \mathbf{K})$ actually mixes the spatial and temporal information on the source in a non-trivial way which depends on the pair velocity $\boldsymbol{\beta}$. Only for time-independent sources things seem to be simple: the correlator then just measures the Fourier transform of the spatial source distribution. Closer inspection shows, however, that it does so only in the directions *perpendicular* to $\boldsymbol{\beta}$ since the time integration leads to a δ -function $\delta(\boldsymbol{\beta}\cdot\mathbf{q})$:

$$\lim_{T \rightarrow \infty} \left| \frac{\int_{-T}^T dt \exp(-i\mathbf{q}\cdot\boldsymbol{\beta}t)}{\int_{-T}^T dt} \right|^2 = \lim_{T \rightarrow \infty} \frac{2\pi}{T} \delta(\mathbf{q}\cdot\boldsymbol{\beta}). \quad (19)$$

This implies that there are no correlations in the direction *parallel* to the pair velocity $\boldsymbol{\beta}$ (which will be called the “outward” direction below), i.e. $C = 1$ for $q_{\text{out}} \neq 0$. The width of the correlator in this direction vanishes! This should puzzle you: wouldn’t you have thought that the width of the correlator in the “outward” direction is inversely related to the source size in that direction (which is, of course, perfectly finite)? As we will see in the next subsection this unexpected behaviour is just another consequence of the mixing of the spatial and temporal structure of the source in the correlator: The width parameter of the correlator in the “outward” direction receives also a contribution from the lifetime of the source which in this case diverges, leading to the vanishing width of the correlator.

It is instructive to look at the problem also in the following way: If one rewrites Eq. (18) in the pair rest frame where $\mathbf{K} = 0$ and hence $q^0 = 0$, one obtains

$$C(\mathbf{q}, \mathbf{K}) - 1 = \int d^3r \cos(\mathbf{q}\cdot\mathbf{r}) S_{\text{rel}}(\mathbf{r}; K) \quad (20)$$

where

$$S_{\text{rel}}(\mathbf{r}; K) = \int d^3R \bar{s}_K(\mathbf{R} + \frac{1}{2}\mathbf{r}) \bar{s}_K(\mathbf{R} - \frac{1}{2}\mathbf{r}), \quad (21)$$

with

$$\bar{s}_K(\mathbf{x}) = \int dt s(\mathbf{x}, t; K) = \int dt \frac{S(x, K)}{\int d^4x' S(x', K)}, \quad (22)$$

is the *time-integrated* normalized relative distance distribution in the source. The latter can, in principle, be uniquely reconstructed from the measured correlator²³ by inverting the cosine-Fourier transform (20). But since it gives

only the time integral of the relative distance distribution for fixed pair momentum \mathbf{K} in the pair rest frame, no direct information on the time structure of the source is obtainable! Only by looking at the result as a function of \mathbf{K} , which, as I will show, brings out the collective dynamical features of the source, can one hope to unfold the time-dependence of the emission function. It is clear that this will be only possible within the context of specific source parametrizations.

2.6 K -dependence of the correlator

We have seen that in general the correlator is a function of *both* \mathbf{q} and \mathbf{K} . Only if the emission function factorizes in x and K , $S(x, K) = F(x) G(K)$, which means that every point x in the source emits particles with the same momentum spectrum $G(K)$ (no “ x - K -correlations”), the K -dependence in $G(K)$ cancels between numerator and denominator of (13), and the correlator seems to be K -independent. However, not even this is really true: even after the cancellation of the explicit K -dependence $G(K)$, there remains an implicit K -dependence via the pair velocity $\beta \approx \mathbf{K}/E_K$ in the exponent on the r.h.s. of Eq. (18)! Only if both conditions, factorization of the emission function in x and K *and* time-independence of the source, apply simultaneously, the correlation function is truly K -independent (because then the β -dependence resides only in the δ -function (19)).

The only practical situation which I know where this occurs and a K -independent correlation function should thus be expected is in HBT interferometry of stars for which the method was invented.²⁴ It is hard to believe that this complication in the application of the original HBT idea to high-energy collisions went nearly unnoticed for more than 20 years and was stumbled upon more or less empirically by Scott Pratt in his pioneering work on HBT interferometry for heavy-ion collisions⁹ only in 1984!

If one parametrises it by a Gaussian in q (see below) this means that in general the parameters (“HBT radii”) depend on K . Typical sources of x - K correlations in the emission function are a collective expansion of the emitter and/or temperature gradients in the particle source: in both cases the momentum spectrum $\sim \exp[-p \cdot u(x)/T(x)]$ of the emitted particles (where $u^\mu(x)$ is the 4-velocity of the expansion flow) depends on the emission point. In the case of collective expansion, the spectra from different emission points are Doppler shifted relative to each other. If there are temperature gradients, e.g. a high temperature in the center and cooler matter at the edges, the source will look smaller for high-momentum particles (which come mostly from the hot center) than for low-momentum ones (which receive larger contributions

also from the cooler outward regions).

We thus see that collective expansion of the source induces a K -dependence of the correlation function. But so do temperature gradients. The crucial question is: does a careful measurement of the correlation function, in particular of its K -dependence, permit a separation of such effects, i.e. can the collective dynamics of the source be quantitatively determined through HBT experiments? We will see that this is not an easy task; however, with sufficiently good data, it should be possible. In any case, the K -dependence of the correlator is a decisive feature which puts the HBT game into a completely new ball park. Two-particle correlation measurements which are not able to resolve the K -dependence of the HBT parameters are, in high energy nuclear and particle physics, of very limited use only. [Unfortunately, this applies to all published HBT data from pp and e^+e^- collisions. In my opinion, a renewed investigation of two-particle correlations from pp and e^+e^- collisions, using the powerful new tool of multidimensional, differential HBT analysis, should be a high priority project – as it is, we have practically nothing with which to compare our heavy-ion results in a meaningful way.]

3 Model-independent discussion of HBT correlation functions

3.1 The Gaussian approximation

The most interesting feature of the two-particle correlation function is its half-width. Actually, since the relative momentum $\mathbf{q} = \mathbf{p}_1 - \mathbf{p}_2$ has three Cartesian components, the fall-off of the correlator for increasing q is not described by a single half-width, but rather by a (symmetric) 3×3 tensor⁸ which describes the curvature of the correlation function near $\mathbf{q} = 0$. We will see that in fact nearly all relevant information that can be extracted from the correlation function resides in the 6 independent components of this tensor. This in turn implies that in order to compute the correlation function C it is sufficient to approximate the source function S by a Gaussian in x which contains only information on its space-time moments up to second order.

Let us write the arbitrary emission function $S(x, K)$ in the following form:

$$S(x, K) = N(K) S(\bar{x}(K), K) e^{-\frac{1}{2} \bar{x}^\mu(K) B_{\mu\nu}(K) \bar{x}^\nu(K)} + \delta S(x, K), \quad (23)$$

where we adjust the parameters $N(K)$, $\bar{x}^\mu(K)$, and $B_{\mu\nu}(K)$ of the Gaussian first term in such a way that the correction term δS has vanishing zeroth, first and second order space-time moments:

$$\int d^4x \delta S(x, K) = \int d^4x x^\mu \delta S(x, K) = \int d^4x x^\mu x^\nu \delta S(x, K) = 0. \quad (24)$$

This is achieved by choosing

$$N(K) = E_K \frac{dN}{d^3K} \frac{\det^{1/2} B_{\mu\nu}(K)}{S(\bar{x}(K), K)}, \quad (25)$$

$$\bar{x}^\mu(K) = \langle x^\mu \rangle, \quad (26)$$

$$(B^{-1})_{\mu\nu}(K) = \langle \tilde{x}_\mu \tilde{x}_\nu \rangle \equiv \langle (x - \bar{x})_\mu (x - \bar{x})_\nu \rangle. \quad (27)$$

The (K -dependent) average over the source function $\langle \dots \rangle$ has been defined in Eq. (13). The normalization factor (25) ensures that the Gaussian term in (23) gives the correct single-particle spectrum (9); it fixes the normalization on-shell, i.e. for $K^0 = E_K$, but as we discussed this is where we need the emission function also for the computation of the correlator. $\bar{x}(K)$ in (26) is the centre of the emission function $S(x, K)$ and approximately equal to its “saddle point”, i.e. the point of highest emissivity for particles with momentum K . The second equality in (27) defines \tilde{x} as the space-time coordinate relative to the centre of the emission function; only this quantity enters the further discussion, since, due to the invariance of the momentum spectra under arbitrary translations of the source in coordinate space, the absolute position of the emission point is not measurable in experiments which determine only particle momenta. Since $\bar{x}(K)$ is not measurable, neither is the normalization $N(K)$ ¹⁴ as its definition (25) involves the emission function at $\bar{x}(K)$. Finally, Eq. (27) ensures that the Gaussian first term in (23) correctly reproduces the second central space-time moments $\langle \tilde{x}_\mu \tilde{x}_\nu \rangle$ of the original emission function, in particular its r.m.s. widths in the various space-time directions.

Inserting the decomposition (23) into Eq. (13) we obtain for the correlation function

$$C(\mathbf{q}, \mathbf{K}) = 1 + \exp[-q^\mu q^\nu \langle \tilde{x}_\mu \tilde{x}_\nu \rangle(\mathbf{K})] + \delta C(\mathbf{q}, \mathbf{K}). \quad (28)$$

The Gaussian in q results from the Fourier transform of the Gaussian contribution in (23); the last term δC receives contributions from the second term δS in (23) which contains information on the third and higher order space-time moments of the emission function, like sharp edges, wiggles, secondary peaks, or non-Gaussian tails in the source. It is at least of fourth order in q , i.e. the second derivative of the full correlator at $q = 0$ is given *exactly* by the Gaussian in (28). Please note that the exponent of the correlator contains no term linear in q ; since the correlator must be symmetric under $\mathbf{q} \rightarrow -\mathbf{q}$ because it does not matter which of the two particles of the pair receives the label 1 or 2, a linear q -dependence could only arise in the form $\exp(-R|q|)$. The only type of emission function yielding such a q -dependence of the correlator would be a spherically symmetric Lorentzian. Any emission function which at large x falls off faster than $1/x^2$ results in the leading Gaussian behaviour (28) instead.

This settles, in my opinion, the old issue whether Gaussian or exponential fits of the correlation function should be preferred.

[In the past it has repeatedly been observed that the correlation data appear to be better fit by exponentials than by Gaussians. However, as far as I know, this happened always when one tried to fit the correlator as a function of the single Lorentz invariant variable $Q_{\text{inv}}^2 = (q^0)^2 - \mathbf{q}^2$. Contemplating the structure of Eq. (28) one realizes that such a fit does not make sense: the generic structure of the exponent, $-q^\mu q^\nu \langle \tilde{x}_\mu \tilde{x}_\nu \rangle$, tells us that the term $(q^0)^2$ should come with the time variance of the source while the spatial components $(q^i)^2$ should come with the spatial variances of the source. Since all variances are positive semidefinite by definition, it does not make sense to parametrize the correlation function by a variable in which $(q^0)^2$ and \mathbf{q}^2 appear with the opposite sign! Such a fit could only work if the time variance and all mixed variances would vanish identically, and all three spatial variances were equal. This is certainly not the general case in nature. The good exponential fits of the correlation functions from pp and e^+e^- collisions are thus, in my mind, purely accidental and an empirical curiosity without physical meaning. *The variable Q_{inv} should not be used for fitting HBT data.*]

Please note also that Eq. (28) has no factor $\frac{1}{2}$ in the exponent. If the measured correlator is fitted by a Gaussian as defined in (28), its q -width can be directly interpreted in terms of the r.m.s. widths of the source in coordinate space. Any remaining factors of $\sqrt{2}$, $\sqrt{3}$, or $\sqrt{5}$ (which you can sometimes find in the literature) are due to reexpressing the r.m.s. width of the source in terms of certain other width parameters chosen for the parametrization of the source in coordinate space. The confusion connected with such factors is easily avoided by always expressing the source parametrization directly in terms of r.m.s. widths.

Eqs. (23) and (28) would, of course, not be useful if the contributions from δS and δC were not somehow small enough to be neglected. This requires a numerical investigation. It was shown¹³ that in typical (and even in some not so typical) situations δS has a negligible influence on the half width of the correlation function. It contributes only weak, essentially unmeasurable structures in $C(\mathbf{q}, \mathbf{K})$ at large values of \mathbf{q} . The reader can easily verify this analytically for an emission function with a sharp box profile; the results⁸ for the exact correlator and the one resulting from the Gaussian approximation (23) differ by less than 5% in the half widths; the exact correlator has, as a function of q , secondary maxima with an amplitude below 5% of the value of the correlator at $q = 0$. We have checked that similar statements remain even true for a source with a doughnut structure, i.e. with a hole in the middle, which was obtained by rotating the superposition of two 1-dimensional

Gaussians separated by twice their r.m.s. widths around their center. The only situation where these statements require qualification is if the correlator receives contributions from the decay of long-lived resonances; unfortunately, this is of relevance for pion interferometry as will be discussed in Sec. refsec6.

From Eq. (28) we conclude that the two-particle correlation function measures the second central space-time moments of the emission function. That's it – finer features of its space-time structure (edges, wiggles, holes) cannot be measured with two-particle correlations, but require the analysis of three-, four-, . . . , many-particle correlations.²⁵ The variances $\langle \tilde{x}_\mu \tilde{x}_\nu \rangle$ are in general *not* identical with our naive intuitive notion of the “source radius”: unless the source is stationary and has no x - K -correlations at all, the variances depend on the momentum \mathbf{K} of the pair and cannot be interpreted in terms of simple overall source geometry. Their correct physical interpretation^{7,10,11} is in terms of “lengths of homogeneity” which give, for each pair momentum \mathbf{K} , the size of the region around the point of maximal emissivity $\bar{x}(\mathbf{K})$ over which the emission function is sufficiently homogeneous to contribute to the correlation function. Thus HBT measures “regions of homogeneity” in the source and their variation with the momentum of the particle pairs. As we will see, the latter is the key to their physical interpretation.

3.2 *YKP parametrization for the correlator and HBT radius parameters*

A full characterization of the source in terms of its second order space-time variances requires knowledge of the 10 parameters $\langle \tilde{x}_\mu \tilde{x}_\nu \rangle$. These quantities appear in the expression (13) for the correlation function but this expression still uses all four components of the relative momentum q^μ . However, as already noted only three of the four components are independent, due to the mass-shell constraint (17). Thus only 6 linear combinations of the variances $\langle \tilde{x}_\mu \tilde{x}_\nu \rangle(\mathbf{K})$ are actually measurable.⁸

If the source is azimuthally symmetric around the beam axis, this counting changes as follows: Even if the source is azimuthally symmetric in coordinate space, the emission function $S(x, K)$ in phase space is for finite \mathbf{K} no longer azimuthally symmetric because the transverse components \mathbf{K}_\perp of the pair momentum distinguish a direction transverse to the beam direction. There remains, however, a reflection symmetry with respect to the plane spanned by \mathbf{K} and the beam axis. If we call the direction orthogonal to this plane y , all mixed variances which are linear in y must vanish due to this reflection symmetry, and the correlator must be symmetric under $q_y \rightarrow -q_y$. Thus only 7 non-vanishing variances $\langle \tilde{x}_\mu \tilde{x}_\nu \rangle$ survive in general, of which, due to the mass-shell constraint (17) only 4 linear combinations are measurable.

Before the correlator (28) can be fit to experimental data, the redundant components of q must first be eliminated from the exponent of the Gaussian via (17). We use a cartesian coordinate system with the z -axis along the beam direction and the x -axis along \mathbf{K}_\perp . Then $\boldsymbol{\beta} = (\beta_\perp, 0, \beta_l)$. We assume an azimuthally symmetric source (impact parameter ≈ 0) and eliminate from (28) q_x and q_y in terms of $q_\perp^2 = q_x^2 + q_y^2$, q_l and q^0 . This yields the YKP parametrization.^{8,14}

$$C(\mathbf{q}, \mathbf{K}) = 1 + \exp \left[-R_\perp^2 q_\perp^2 - R_\parallel^2 (q_l^2 - (q^0)^2) - (R_0^2 + R_\parallel^2) (q \cdot U)^2 \right]. \quad (29)$$

Here R_\perp , R_\parallel , R_0 , U are four K -dependent parameter functions. $U(\mathbf{K})$ is a 4-velocity with only a longitudinal spatial component:

$$U(\mathbf{K}) = \gamma(\mathbf{K}) (1, 0, 0, v(\mathbf{K})), \quad \text{with } \gamma = \frac{1}{\sqrt{1 - v^2}}. \quad (30)$$

Its value depends, of course, on the measurement frame. The ‘‘Yano-Koonin velocity’’ $v(\mathbf{K})$ can be calculated¹⁴ in an arbitrary reference frame from the second central space-time moments of $S(x, K)$. It is, to a good approximation, the longitudinal velocity of the fluid element from which most of the particles with momentum \mathbf{K} are emitted.^{8,14} For sources with boost-invariant longitudinal expansion velocity the YK-rapidity associated with $v(\mathbf{K})$ is linearly related to the pair rapidity Y .¹⁴

The other three YKP parameters do not depend on the longitudinal velocity of the observer. (This distinguishes the YKP form (29) from the Pratt-Bertsch parametrization^{6,7,9} which results from eliminating q^0 in (28).) Their physical interpretation is easiest in terms of coordinates measured in the frame where $v(\mathbf{K})$ vanishes. There they are given by⁸

$$R_\perp^2(\mathbf{K}) = \langle \tilde{y}^2 \rangle, \quad (31)$$

$$R_\parallel^2(\mathbf{K}) = \left\langle (\tilde{z} - (\beta_l/\beta_\perp)\tilde{x})^2 \right\rangle - (\beta_l/\beta_\perp)^2 \langle \tilde{y}^2 \rangle \approx \langle \tilde{z}^2 \rangle, \quad (32)$$

$$R_0^2(\mathbf{K}) = \left\langle (\tilde{t} - \tilde{x}/\beta_\perp)^2 \right\rangle - \langle \tilde{y}^2 \rangle / \beta_\perp^2 \approx \langle \tilde{t}^2 \rangle. \quad (33)$$

R_\perp , R_\parallel and R_0 thus measure, approximately, the (K -dependent) transverse, longitudinal and temporal regions of homogeneity of the source in the local co-moving frame of the emitter. The approximation in (32,33) consists of dropping terms which for the model discussed below vanish in the absence of transverse flow and were found to be small even for finite transverse flow.¹⁴ Note that it leads to a complete separation of the spatial and temporal aspects of the

source. This separation is spoiled by sources with $\langle \tilde{x}^2 \rangle \neq \langle \tilde{y}^2 \rangle$. For our source this happens for non-zero transverse (in particular for large) transverse flow η_f , but for opaque sources where particle emission is surface dominated²⁶ this occurs even without transverse flow.^{26,27}

4 A model for a finite expanding source

For our quantitative studies we used the following model for an expanding thermalized source⁸

$$S(x, K) = \frac{M_{\perp} \cosh(\eta - Y)}{8\pi^4 \Delta\tau} \exp\left[-\frac{K \cdot u(x)}{T(x)} - \frac{(\tau - \tau_0)^2}{2(\Delta\tau)^2} - \frac{r^2}{2R^2} - \frac{(\eta - \eta_0)^2}{2(\Delta\eta)^2}\right] \quad (34)$$

Here $r^2 = x^2 + y^2$, the spacetime rapidity $\eta = \frac{1}{2} \ln[(t+z)/(t-z)]$, and the longitudinal proper time $\tau = \sqrt{t^2 - z^2}$ parametrize the spacetime coordinates x^μ , with measure $d^4x = \tau d\tau d\eta r dr d\phi$. $Y = \frac{1}{2} \ln[(E_K + K_L)/(E_K - K_L)]$ and $M_{\perp} = \sqrt{m^2 + K_{\perp}^2}$ parametrize the longitudinal and transverse components of the pair momentum \mathbf{K} . $\sqrt{2}R$ is the transverse geometric (Gaussian) radius of the source, τ_0 its average freeze-out proper time, $\Delta\tau$ the mean proper time duration of particle emission, and $\Delta\eta$ parametrizes the finite longitudinal extension of the source. $T(x)$ is the freeze-out temperature; if you don't like the idea of thermalization in heavy ion collisions, you can think of it as a parameter that describes the random distribution of the particle momenta at each space-time point around their average value. The latter is parametrized by a collective flow velocity $u^\mu(x)$ in the form

$$u^\mu(x) = (\cosh \eta \cosh \eta_t(r), \sinh \eta_t(r) \mathbf{e}_r, \sinh \eta \cosh \eta_t(r)), \quad (35)$$

with a boost-invariant longitudinal flow rapidity $\eta_t = \eta$ ($v_l = z/t$) and a linear transverse flow rapidity profile

$$\eta_t(r) = \eta_f \left(\frac{r}{R}\right). \quad (36)$$

η_f scales the strength of the transverse flow. The exponent of the Boltzmann factor in (34) can then be written as

$$K \cdot u(x) = M_{\perp} \cosh(Y - \eta) \cosh \eta_t(r) - \mathbf{K}_{\perp} \cdot \mathbf{e}_r \sinh \eta_t(r). \quad (37)$$

For vanishing transverse flow ($\eta_f = 0$) the source depends only on M_{\perp} , and remains azimuthally symmetric for all K_{\perp} . Since in the absence of transverse flow the β -dependent terms in (32) and (33) vanish and the source itself depends

only on M_{\perp} , all three YKP radius parameters then show perfect M_{\perp} -scaling. Plotted as functions of M_{\perp} , they coincide for pion and kaon pairs (see Fig. 1, left column). For non-zero transverse flow (right column) this M_{\perp} -scaling is broken by two effects: (1) The thermal exponent (37) receives an additional contribution proportional to $K_{\perp} = \sqrt{M_{\perp}^2 - m^2}$. (2) The terms which were neglected in the second equalities of (32,33) are non-zero, and they also depend on $\beta_{\perp} = K_{\perp}/E_K$. Both effects induce an explicit rest mass dependence and destroy the M_{\perp} -scaling of the YKP size parameters.

5 K -dependence of YKP parameters and collective flow

Collective expansion induces correlations between coordinates and momenta in the source, and these result in a dependence of the HBT parameters on the pair momentum K . At each point in the source the local velocity distribution is centered around the average fluid velocity; two points whose fluid elements move rapidly relative to each other are thus unlikely to contribute particles with small relative momenta. Essentially only such regions in the source contribute to the correlation function whose fluid elements move with velocities close to the velocity of the observed particle pair.

5.1 The Yano-Koonin velocity and longitudinal flow

Fig. 2 shows (for pion pairs) the dependence of the YK velocity on the pair momentum \mathbf{K} . In Fig. 2a we show the YK rapidity $Y_{\text{YK}} = \frac{1}{2} \ln[(1+v)/(1-v)]$ as a function of the pair rapidity Y (both relative to the CMS) for different values of K_{\perp} , in Fig. 2b the same quantity as a function of K_{\perp} for different Y . Solid lines are without transverse flow, dashed lines are for $\eta_f = 0.6$. For large K_{\perp} pairs, the YK rest frame approaches the LCMS (which moves with the pair rapidity Y); in this limit all pairs are thus emitted from a small region in the source which moves with the same longitudinal velocity as the pair. For small K_{\perp} the YK frame is considerably slower than the LCMS; this is due to the thermal smearing of the particle velocities in our source around the local fluid velocity $u^{\mu}(x)$.¹⁴ The linear relationship between the rapidity Y_{YK} of the Yano-Koonin frame and the pion pair rapidity Y is a direct reflection of the boost-invariant longitudinal expansion flow.¹⁴ For a non-expanding source Y_{YK} would be independent of Y . Additional transverse flow is seen to have nearly no effect. The dependence of the YK velocity on the pair rapidity thus measures directly the longitudinal expansion of the source and cleanly separates it from its transverse dynamics.

The NA49 data for 160 A GeV Pb+Pb collisions^{28,29} show very clearly

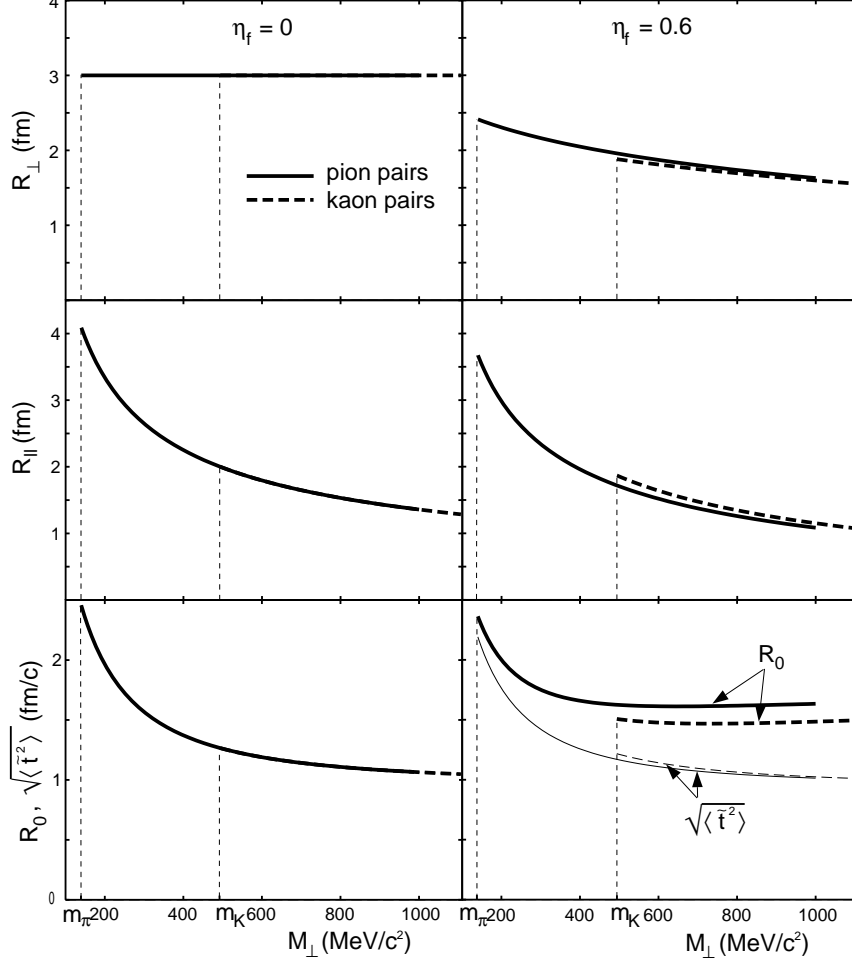


Figure 1: The YKP radii R_{\perp} , R_{\parallel} , and R_0 (top to bottom) for zero transverse flow (left column) and for $\eta_f = 0.6$ (right column), as functions of M_{\perp} for pairs at $Y_{\text{cm}} = 0$. Solid (dashed) lines are for pions (kaons). The breaking of the M_{\perp} -scaling by transverse flow is obvious in the right column. For nonzero transverse flow R_0 also does not agree exactly with the effective source lifetime $\sqrt{\langle \tilde{t}^2 \rangle}$ (lower right panel). Source parameters: $T = 140$ MeV, $\Delta\eta = 1.2$, $R = 3$ fm, $\tau_0 = 3$ fm/c, $\Delta\tau = 1$ fm/c.

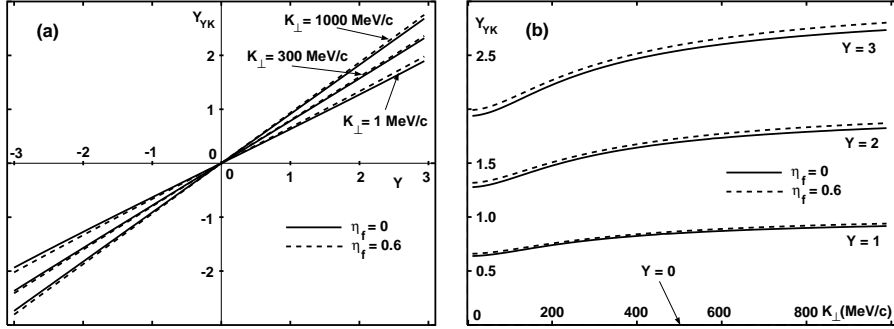


Figure 2: (a) The Yano-Koonin rapidity for pion pairs, as a function of the pair c.m. rapidity Y , for various values of K_{\perp} and two values for the transverse flow η_f . (b) The same, but plotted against K_{\perp} for various values of Y and η_f . Source parameters as in Fig. 1.

such a more or less linear rise of the Yano-Koonin source rapidity with the rapidity of the pion pair. This confirms, in the most transparent way imaginable, their earlier conclusion³⁰ based on the Y -dependence of the longitudinal radius parameter R_l in the Pratt-Bertsch parametrization that the source created in 200 A GeV S+A collisions expands longitudinally in a nearly boost-invariant way.

It should be noted that this longitudinal flow need not be of hydrodynamical (pressure generated) nature. In a description of nuclear collisions as a set of longitudinally oriented and independently fragmenting nucleon-nucleon strings, the string fragmentation process would also lead to a strong correlation between the longitudinal positions and momenta of the created hadrons. Thus a similar linear rise of the YK-rapidity with the pair rapidity would be expected in jet fragmentation (with the z -axis oriented along the jet axis). It would be interesting to confirm this prediction in e^+e^- or pp collisions.

5.2 M_{\perp} -dependence of YKP radii; transverse flow

If the source expands rapidly and features large velocity gradients, the “regions of homogeneity” contributing to the correlation function will be small. Their size will be inversely related to the velocity gradients, scaled by a “thermal smearing factor” $\sqrt{T/M_{\perp}}$ which characterizes the width of the Boltzmann distribution.⁷ If one evaluates the expectation values (31-33) by saddle point

integration one finds for pairs with $Y = 0$

$$R_{\perp}^2 = R_*^2, \quad (38)$$

$$R_0^2 = (\Delta t_*)^2, \quad (39)$$

$$R_{\parallel}^2 = L_*^2, \quad (40)$$

with

$$\frac{1}{R_*^2} = \frac{1}{R^2} + \frac{1}{R_{\text{flow}}^2}, \quad (41)$$

$$(\Delta t_*)^2 = (\Delta\tau)^2 + 2 \left(\sqrt{\tau_0^2 + L_*^2} - \tau_0 \right)^2, \quad (42)$$

$$\frac{1}{L_*^2} = \frac{1}{(\tau_0 \Delta\eta)^2} + \frac{1}{L_{\text{flow}}^2}, \quad (43)$$

where R_{flow} and L_{flow} are the transverse and longitudinal “dynamical lengths of homogeneity” due to the expansion velocity gradients:

$$R_{\text{flow}}(M_{\perp}) = \frac{R}{\eta_f} \sqrt{\frac{T}{M_{\perp}}} = \frac{1}{\partial\eta_t(r)/\partial r} \sqrt{\frac{T}{M_{\perp}}}, \quad (44)$$

$$L_{\text{flow}}(M_{\perp}) = \tau_0 \sqrt{\frac{T}{M_{\perp}}} = \frac{1}{\partial \cdot u_l} \sqrt{\frac{T}{M_{\perp}}}, \quad (45)$$

where u_l is the longitudinal 4-velocity.

Thus, for expanding sources, the HBT radius parameters are generically decreasing functions of the transverse pair mass M_{\perp} . The slope of this decrease grows with the expansion rate^{13,14} (this cannot be seen in the saddle point approximated expressions above). Longitudinal expansion affects mostly the longitudinal radius parameter R_{\parallel} and the temporal parameter R_0 ;¹⁴ the latter is a secondary effect since particles from different points are usually emitted at different times, and a decreasing longitudinal homogeneity length thus also leads to a reduced effective duration of particle emission (see lower panels in Fig. 1). The transverse radius parameter R_{\perp} is invariant under longitudinal boosts and thus not affected at all by longitudinal expansion (upper left panel in Fig. 1). It begins to drop as a function of M_{\perp} , however, if the source expands in the transverse directions (upper right panel). Comparing the lower two left and right panels in Fig. 1 one sees that the sensitivity of R_{\parallel} and R_0 to transverse flow is much weaker.¹⁴ Transverse (longitudinal) flow thus affects mostly the transverse (longitudinal) regions of homogeneity.

While longitudinal “flow” is not necessarily a signature for nuclear collectivity but could be “faked” as discussed at the end of the previous subsection, transverse flow is much more generic in this respect: there is clearly no transverse collective dynamics in the ingoing channel, and the only mechanism imaginable for the creation of transverse flow is multiple (re-)scattering among the participants and secondaries, leading ultimately to hydrodynamic transverse expansion.

Unfortunately, the observation of an M_{\perp} -dependence of R_{\perp} by itself is not sufficient to prove the existence of radial transverse flow. It can also be created by other types of transverse gradients, e.g. a transverse temperature gradient.^{7,12,27} To exclude such a possibility one must check the M_{\perp} -scaling of the YKP radii, i.e. the independence of the functions $R_i(M_{\perp})$ ($i = \perp, \parallel, 0$) of the particle rest mass (which is not broken by temperature gradients). Since different particle species are affected differently by resonance decays, such a check further requires the elimination of resonance effects.

6 Resonance decays

Resonance decays contribute additional pions at low M_{\perp} ; these pions originate from a larger region than the direct ones, due to resonance propagation before decay. They cause an M_{\perp} -dependent modification of the HBT radii.

Quantitative studies^{15,16} have shown that the resonances can be subdivided into three classes with different characteristic effects on the correlator: (i) Short-lived resonances with lifetimes up to a few fm/c do not propagate far outside the region of thermal emission and thus affect R_{\perp} only marginally. They contribute to R_0 and R_{\parallel} up to about 1 fm via their lifetime; R_{\parallel} is larger if pion emission occurs later because for approximately boost-invariant expansion the longitudinal velocity gradient decreases as a function of time.

(ii) Long-lived resonances with lifetimes of more than several hundred fm/c do not contribute to the measurable correlation and thus only reduce the correlation strength (the intercept at $q = 0$), without changing the shape of the correlator.^a The reason is that they propagate very far before decaying, thus simulating a very large source which contributes to the correlation signal only for unmeasurably small relative momenta.

(iii) There is only one resonance which does not fall in either of these two classes and can thus distort the form of the correlation function: the ω with

^aA reduced correlation strength in the two-particle sector could also arise from partial phase coherence in the source.³¹ By comparing two- and three-particle correlations, the intercept reducing effects of resonances can be eliminated, and the degree of coherence resp. chaoticity in the source can be unambiguously determined.²⁵

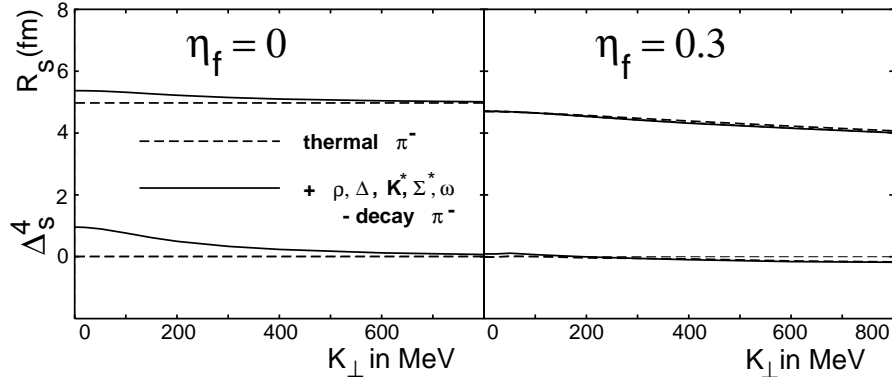


Figure 3: The inverted q -variance R_{\perp} and the kurtosis Δ_{\perp} (the index s in the figure stands for “sideward”) at $Y = 0$ as functions of K_{\perp} . Left: $\eta_f = 0$ (no transverse flow). Right: $\eta_f = 0.3$. The difference between dashed and solid lines is entirely dominated by ω decays. Source parameters as in Fig. 1, except for $R = 5$ fm.

its lifetime of 23.4 fm/ c . It contributes a second bump at small q to the correlator, giving it a non-Gaussian shape and complicating¹⁶ the extraction of HBT radii by a Gaussian fit to the correlation function. At small M_{\perp} up to 10% of the pions can come from ω decays, and this fraction doubles effectively in the correlator since the other pion can be a direct one; thus the effect is not always negligible.

In a detailed model study¹⁶ we showed that resonance contributions can be identified through the non-Gaussian features in the correlator induced by the tails in the emission function resulting from resonance decays. To this end one computes the second and fourth order q -moments of the correlator.¹⁶ The second order moments define the HBT radii, while the kurtosis (the normalized fourth order moments) provide a lowest order measure for the deviations from a Gaussian shape. We found¹⁶ that, at least for the model (34), a positive kurtosis can always be associated with resonance decay contributions (Fig. 3, left panel). Strong flow also generates a non-zero, but small and apparently always negative kurtosis (Fig. 3, right panel). Any M_{\perp} -dependence of R_{\perp} which is associated with a positive M_{\perp} -dependent kurtosis must therefore be regarded with suspicion; an M_{\perp} -dependence of R_{\perp} with a vanishing or negative kurtosis, however, cannot be blamed on resonance decays.

In our model, the first situation is realized for a source without transverse expansion (left panel of Fig. 1): At small M_{\perp} the ω contribution increases R_{\perp} by up to 0.5 fm while for $M_{\perp} > 600$ MeV it dies out. The effect on R_{\perp}

is small because the heavy ω moves slowly and doesn't travel very far before decaying. The resonance contribution is clearly visible in the positive kurtosis (lower curve). For non-zero transverse flow (right panel) there is no resonance contribution to R_{\perp} ; this is because for finite flow the effective source size for the heavier ω is smaller than for the direct pions, and the ω -decay pions thus always remain buried under the much more abundant direct ones. Correspondingly the kurtosis essentially vanishes; in fact, it is slightly negative, due to the weak non-Gaussian features induced by the transverse flow.

7 Opaque sources

The emission function (34) is only one of an infinity of possible source parametrizations. It is chosen in such a way that it allows easy implementation of most features which we believe are important for the sources created in heavy ion collisions. There is, however, one important physical situation which cannot be parametrized in any reasonable way by the formula (34): if the source emits particles not from the entire volume, but only from a thin surface layer. This is how the sun radiates photons, and this is also an often suggested picture for the case that a QGP is created in the collision which then hadronizes slowly in a deflagration-type strong first order transition by surface emission of hadrons from the edge of the QGP blob.

The significance of such a phenomenon for HBT interferometry was realized by Heiselberg and Vischer²⁶ who pointed out that an effective emission region which is part of a thin surface layer has a much smaller extension in the “outward” or x -direction than in the “sideward” or y -direction. In other words, such “opaque sources” have $\langle \tilde{x}^2 - \tilde{y}^2 \rangle < 0$. Depending on the degree of opacity (the thickness of the surface layer relative to the source radius) this difference can be large and negative. The authors pointed out²⁶ that this leads to the possibility of a smaller “outward” than “sideward” HBT radius parameter in the Pratt-Bertsch parametrization, even at $K_{\perp} = 0$. Recently B. Tomášik showed²⁷ that in the YKP parametrization opacity effects would show up even more spectacularly by a “lifetime parameter” R_0^2 which would diverge to $-\infty$ in the limit $K_{\perp} \rightarrow 0$ resp. $\beta_{\perp} \rightarrow 0$ (see Eq. (33)).

The source (34) can be made opaque by multiplying it by the factor^{26,27}

$$\exp\left(-\kappa \frac{l_{\text{eff}}}{\lambda}\right) \quad (46)$$

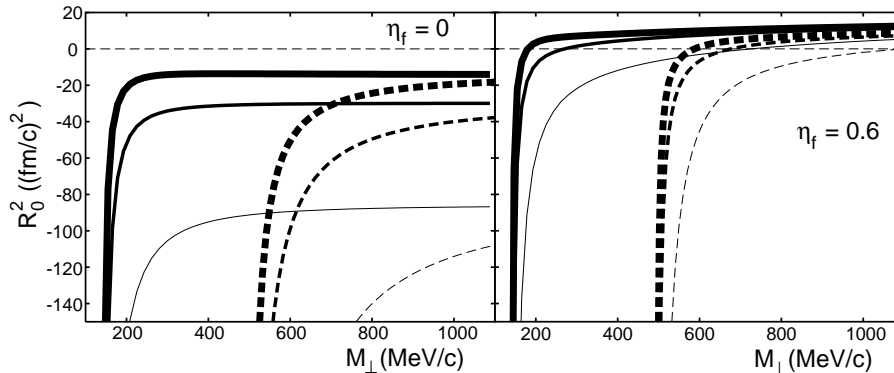


Figure 4: The YKP parameter $R_0^2(M_\perp)$ for midrapidity pairs for various combinations of λ and η_f . Solid (dashed) lines are for pions (kaons). Thin lines: $\lambda = 1 \text{ fm} = R/7$; medium lines: $\lambda = 7 \text{ fm} = R$; thick lines: $\lambda = 14 \text{ fm} = 2R$. Left: $\eta_f = 0$; right: $\eta_f = 0.6$. Source parameters: $T = 100 \text{ MeV}$, $\Delta\eta = 1.3$, $\tau_0 = 7.8 \text{ fm}/c$, $\Delta\tau = 2 \text{ fm}/c$, $R = 7 \text{ fm}$.

where λ is the mean free path,

$$l_{\text{eff}} = l_{\text{eff}}(r, \phi) = e^{-\frac{y^2}{2R^2}} \int_x^\infty e^{-\frac{x'^2}{2R^2}} dx' \quad \text{with } y = r \sin \phi, x = r \cos \phi. \quad (47)$$

is the effective travelling distance of the emitted particle through matter in the source (34), and $\kappa = \sqrt{8/\pi}$ is a parameter which is adjusted in such a way that particles emitted from the center suffer the same suppression as in the model of Heiselberg and Vischer²⁶ who use a box distribution instead of the Gaussians in (34).

Fig. 4 shows the interesting YKP parameter, the “temporal” radius parameter R_0^2 , as a function of M_\perp for sources with different degrees of opacity. With or without transverse flow, the crucial features of opacity are clearly visible: the negative contribution $\sim \langle \tilde{x}^2 - \tilde{y}^2 \rangle$ in (33) drives R_0^2 to negative values at small K_\perp , and this happens the sooner the shorter the mean free path λ , i.e. the thinner the surface layer is.

Comparing the solid curves for pion pairs in Fig. 4 with the Pb+Pb data²⁹ in Fig. 5 below I conclude that mean free path values $\lambda < R$ are essentially excluded. (This conclusion has in the meantime been checked by more extensive parameter studies.) In other words, the sources created in 160 A GeV Pb+Pb collisions are not at all opaque, but rather “transparent”, meaning that particles are emitted from the whole volume by bulk rather than surface dominated freeze-out.

8 Analysis of Pb+Pb data

In Fig. 5 we show a numerical fit of the YKP radius parameters, using the expressions (31)-(33) with our model source (34), to data collected by the NA49 collaboration in 158 A GeV/c Pb+Pb collisions.^{28,29} Please note that this fit refers to only a single rapidity slice of the available data, and it does not include resonance decays (although we do not expect the latter to change things much, except for reducing τ_0 by about 1 fm/c, the average lifetime of the shortlived resonances, see Sec. 6). The fit result must therefore be taken with some care. A comprehensive simultaneous analysis of all single particle spectra and two-particle correlation data from Pb+Pb collisions is in progress.

After $\Delta\eta=1.3$ has been adjusted to reproduce the width of the pion rapidity distribution,²⁹ the parameters τ_0 and $\Delta\eta$ are essentially fixed by the magnitude of R_{\parallel} and R_0 . The radius R is fixed by the magnitude of $R_{\perp}(K_{\perp} = 0)$ once the temperature T and transverse flow η_f are known. The M_{\perp} -dependence of R_{\perp} fixes T and η_f , albeit not independently: essentially only the combination $\eta_f\sqrt{M_{\perp}/T}$, i.e. the velocity gradient divided by the thermal smearing factor, can be extracted.^{8,29} This is similar to the single particle spectra whose M_{\perp} -slopes determine only an effective blushifted temperature,¹ $T_{\text{eff}} = T\sqrt{\frac{1+\bar{v}_f}{1-\bar{v}_f}}$. The correlations between T and η_f are, however, exactly opposite in the two cases: for a fixed spectral slope T must be decreased if η_f increases while a fixed M_{\perp} -slope of R_{\perp} requires decreasing values of η_f if T is reduced.²⁹ *The combination of single-particle spectra and two-particle correlation thus allows for a separate determination of T and η_f .*

For the fit in Fig. 5 the freeze-out temperature was set by hand to $T = 100$ MeV. The resulting flow parameter $\eta_f=0.6$ corresponds to an average transverse flow velocity $\bar{v}_f=0.58$. This combination of T and η_f results in single-particle spectra with roughly the right shape. Somewhat higher temperature values of around $T = 120$ MeV as advocated by Kämpfer³² with an average transverse flow velocity $\bar{v}_f = 0.43 c$ produce a somewhat flatter decrease of R_{\perp} with M_{\perp} but still appear to be consistent with the data inside the error bars. Fitting R_{\perp} with even higher temperatures results in larger η_f -values which leads to single particle spectra which are much too flat.

Let us discuss in more detail the numbers resulting from this fit. First, the transverse size parameter $R=7$ fm is surprisingly large. Resonance contributions are not expected to reduce it by more than 0.5 fm.¹⁶ The transverse flow correction to R_{\perp} is appreciable, resulting in a visible transverse homogeneity length of only about 5.5 fm at small K_{\perp} , but even this number is large. $R=7$ fm corresponds to an r.m.s. radius $r_{\text{rms}} = \sqrt{\langle \tilde{x}^2 + \tilde{y}^2 \rangle} \approx 10$ fm of the pion source,

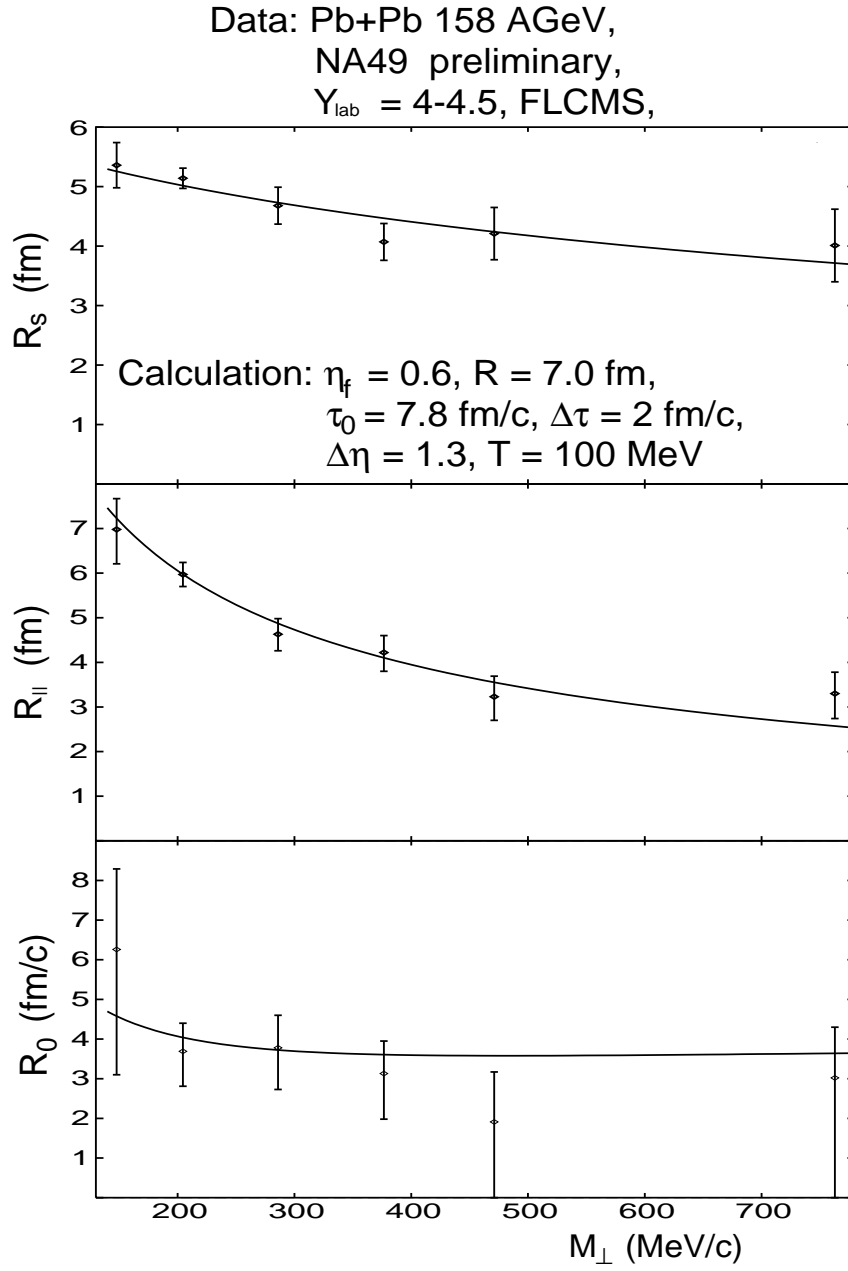


Figure 5: R_{\perp} , $R_{||}$ and R_0 for 158 A GeV/c Pb+Pb collisions as functions of the transverse pair momentum. The data are from the NA49 Collaboration.²⁹ The lines are a fit with the model (34), with fit parameters as given in the figure.

to be compared with an r.m.s. radius $r_{\text{rms}}^{\text{Pb}} = 1.2 \times A^{1/3} * \sqrt{2/5} \text{ fm} = 4.5 \text{ fm}$ for the density distribution of the original Pb nucleus projected on the transverse plane.^b This implies a transverse expansion of the reaction zone by a linear factor $10/4.5 = 2.2$. That we also find a large transverse flow velocity renders the picture consistent. The longitudinal size of the collision region at the point where the pressure in the system began to drive the transverse expansion can be estimated as follows: for the source to expand in, say, the y -direction from $\sqrt{\langle y^2 \rangle}_{\text{initial}} = 1.2 A^{1/3} / \sqrt{5} \text{ fm} = 3.2 \text{ fm}$ to $\sqrt{\langle y^2 \rangle}_{\text{final}} = R = 7 \text{ fm}$ with an average transverse flow velocity of at most $\bar{v} = 0.58 c$ (the freeze-out value determined from the fit of R_{\perp}) requires at time of at least $(7 - 3.2)/0.58 \text{ fm}/c = 6.5 \text{ fm}/c$. Due to the selfsimilarity of the longitudinal expansion the longitudinal dimension of the source grows linearly with τ . If the total expansion time until freeze-out is given by the fit parameter $\tau_0 = 7.8 \text{ fm}/c$, the source expanded in the $6.5 \text{ fm}/c$ during which there was transverse expansion by a factor $7.8/(7.8-6.5) = 7.8/1.3 = 6$ in the longitudinal direction. We conclude that the fireball volume must have expanded by a factor $6 * 2.2^2 \approx 30$ between the onset of transverse expansion and freeze-out! This is the clearest evidence for strong collective dynamical behaviour in ultra-relativistic heavy-ion collisions so far.

The local comoving energy density at freeze-out can be estimated from the fitted values for T and η_f . The thermal energy density of a hadron resonance gas at $T = 100 \text{ MeV}$ and moderate baryon chemical potential is of the order of $50 \text{ MeV}/\text{fm}^3$. The large average transverse flow velocity of $\langle v_f \rangle \approx 0.58$ implies that about 50% flow energy must be added in the lab frame. This results in an estimate of about $0.050 \text{ GeV}/\text{fm}^3 \times 1.5 \times 30 \approx \mathbf{2.2 \text{ GeV}/\text{fm}^3}$ for the energy density of the reaction zone at the onset of transverse expansion. This is well above the critical energy density $\epsilon_{\text{cr}} \leq 0.9 \text{ GeV}/\text{fm}^3$ predicted by lattice QCD for deconfined quark-gluon matter.³⁴ Whether this energy density was fully thermalized is, of course, a different question. It must, however, have been accompanied by transverse pressure (i.e. some degree of equilibration of momenta must have occurred already before this point), because otherwise transverse expansion could not have been initiated.

9 Conclusions

I hope to have shown that

^bIn my lecture given at the workshop I made an embarrassing error by a factor $\sqrt{2}$ which is also contained in the writeup³³ of my talk at Hirscheegg in January 1996. I would like to thank D. Ferenc for pointing out this error.

- two-particle correlation functions from heavy-ion collisions provide valuable information both on the geometry **and** the dynamical state of the reaction zone at freeze-out;
- a comprehensive and simultaneous analysis of single-particle spectra and two-particle correlations, with the help of models which provide a realistic parametrization of the emission function, allows for an essentially complete reconstruction of the final state of the reaction zone, which can serve as a reliable basis for theoretical back-extrapolations towards the interesting hot and dense early stages of the collision;
- simple and conservative estimates, based on the crucial new information from HBT measurements on the large transverse size of the source at freeze-out and using only energy conservation, lead to the conclusion that in Pb+Pb collisions at CERN, before the onset of transverse expansion, the energy density exceeded comfortably the critical value for the formation of a color deconfined state of quarks and gluons. There is, however, no evidence for long time delays due to hadronization of the QGP, and pion freeze-out occurs in bulk rather than from the surface of the collision fireball. This is in line with lattice results which predict at most a *weakly* first order confinement transition, and with other evidence³⁵ for rapid hadronization.

Acknowledgements:

This work was supported by grants from DAAD, DFG, NSFC, BMBF and GSI. The results reported here were obtained in collaboration with D. Anchishkin, S. Chapman, P. Scotto, B. Tomášik, U. Wiedemann, and Y.-F. Wu, to whom I would like express my thanks. I gratefully acknowledge many discussions with H. Appelshäuser, T. Csörgő, D. Ferenc, M. Gaździcki, S. Schönfelder, P. Seyboth, and A. Vischer.

References

1. K.S. Lee and U. Heinz, *Z. Phys. C* **43**, 425 (1989); K.S. Lee, U. Heinz and E. Schnedermann, *Z. Phys. C* **48**, 525 (1990); E. Schnedermann and U. Heinz, *Phys. Rev. Lett.* **69**, 2908 (1992); E. Schnedermann, J. Sollfrank and U. Heinz, *Phys. Rev. C* **48**, 2462 (1993); E. Schnedermann and U. Heinz, *Phys. Rev. C* **50**, 1675 (1994); U. Heinz, in *Hot Hadronic Matter: Theory and Experiment*, (J. Letessier *et al.*, eds.), NATO ASI Series **B346** (Plenum, New York, 1995), p. 413.

2. J. Stachel *et al.*, [E814 collaboration], *Nucl. Phys. A* **566**, 183c (1994); P. Braun-Munzinger *et al.*, *Phys. Lett. B* **344**, 43 (1995).
3. See proceedings of *Quark Matter 96*, *Nucl. Phys. A* **610** (1996), in particular contributions by Y. Akiba, N. Herrmann, P. Jones, R. Lacasse, J. Stachel, and Nu Xu.
4. A. Leonidov, M. Nardi and H. Satz, *Z. Phys. C* **74**, 535 (1997).
5. S. Esumi, U. Heinz, and N. Xu, *Phys. Lett. B* **409**, 479 (1997).
6. M. Herrmann and G.F. Bertsch, *Phys. Rev. C* **51**, 328 (1995).
7. S. Chapman, P. Scotto and U. Heinz, *Phys. Rev. Lett.* **74**, 4400 (1995); and *Heavy Ion Physics* **1**, 1 (1995).
8. S. Chapman, J.R. Nix and U. Heinz, *Phys. Rev. C* **52**, 2694 (1995).
9. S. Pratt, *Phys. Rev. Lett.* **53**, 1219 (1984); *Phys. Rev. D* **33**, 1314 (1986).
10. A.N. Makhlin and Yu.M. Sinyukov, *Z. Phys. C* **39**, 69 (1988).
11. S.V. Akkelin and Y.M. Sinyukov, *Phys. Lett. B* **356**, 525 (1995).
12. T. Csörgő and B. Lörstad, *Phys. Rev. C* **54**, 1396 (1996).
13. U.A. Wiedemann, P. Scotto and U. Heinz, *Phys. Rev. C* **53**, 918 (1996).
14. U. Heinz *et al.*, *Phys. Lett. B* **382**, 181 (1996); Wu Y.-F. *et al.*, *Z. Phys. C* **77** (1996), in press (nucl-th/9607044).
15. B.R. Schlei *et al.*, *Phys. Lett. B* **293**, 275 (1992); J. Bolz *et al.*, *ibid.* **300**, 404 (1993); *Phys. Rev. D* **47**, 3860 (1993).
16. U.A. Wiedemann and U. Heinz, *Phys. Rev. C* **56**, R610 (1997); and *Phys. Rev. C* **56** (1. Dec. 1997) (nucl-th/9611031)
17. U. Heinz, in *Correlations and Clustering Phenomena in Subatomic Physics*, (M.N. Harakeh *et al.*, eds.), NATO ASI Series **B359** (Plenum, New York, 1997), p. 137.
18. M. Gyulassy, S.K. Kauffmann, and L.W. Wilson, *Phys. Rev. C* **20**, 2267 (1979).
19. E. Shuryak, *Phys. Lett. B* **44**, 387 (1973); *Sov. J. Nucl. Phys.* **18**, 667 (1974).
20. S. Chapman and U. Heinz, *Phys. Lett. B* **340**, 250 (1994).
21. D. Anchishkin, U. Heinz, and P. Renk, nucl-th/9710051, submitted to *Phys. Rev. C*.
22. Q.H. Zhang, U.A. Wiedemann, C. Slotta, and U. Heinz, *Phys. Lett. B* **407**, 33 (1997).
23. D.A. Brown and P. Danielewicz, *Phys. Lett. B* (1997), in press (nucl-th/9701010).
24. R. Hanbury Brown and R.Q. Twiss, *Phil. Mag.* **45**, 633 (1954); and *Nature* **177**, 27 (1965); **178**, 1046 and 1447 (1956).
25. U. Heinz and Q.H. Zhang, *Phys. Rev. C* **56**, 426 (1997).

26. H. Heiselberg and A.P. Vischer, *Z. Phys. C* (1997), in press.
27. B. Tomášik and U. Heinz, nucl-th/9707001.
28. NA49 Coll., K. Kadija *et al.*, *Nucl. Phys. A* **610**, 248c (1996); H. Appelshäuser, PhD thesis, Univ. Frankfurt (1996).
29. S. Schönfelder, PhD thesis, MPI für Physik, München (1996).
30. T. Alber *et al.*, *Z. Phys. C* **66**, 77 (1995).
31. I.V. Andreev, M. Plümer, and R.M. Weiner, *Int. J. Mod. Phys. A* **8**, 4577 (1993).
32. B. Kämpfer, nucl-th/9612336, and private communication.
33. U. Heinz, in *QCD phase transitions*, (H. Feldmeier *et al.*, eds.), GSI Report ISSN 0720-8715, March 1997, p. 361.
34. F. Karsch, lectures given at Kloster Banz, Oct. 8-10, 1996; E. Laermann, *Nucl. Phys. A* **610**, 1c (1996).
35. J. Letessier, A. Tounsi, U. Heinz, J. Sollfrank, and J. Rafelski, *Phys. Rev. C* **51**, 3408 (1995).